A Demodulation Technique for Spindle Rotor Position Detection With Resolver

Nay Lin Htun Aung[1], Chao Bi[1], Abdullah Al Mamun[2], Cheng Su Soh[1], and Yu YinQuan[1]

[1]Data Storage Institute, 117608 Singapore

[2]Department of Electrical and Computer Engineering, National University of Singapore, 117583 Singapore

This paper presents a demodulation technique for amplitude modulated signals from a resolver based on amplitude detection of a sinusoidal waveform by numerical integration. The proposed technique performs synchronous integration on output signals of the resolver. The integration period is determined from zero crossing detection of the same output signals. The actual envelopes of the signal waveforms are obtained by utilizing the phase relationship of the integrated waveforms with the delayed carrier signal. Due to integration, the noise and disturbance effects are averaged out and the achievable accuracy is improved without applying filters. The method is developed from exploration of detecting HDD spindle rotor position in high resolution. The effectiveness of the proposed technique is demonstrated with the simulations and compared to the other methods. Experimental results are also provided to support the proposed method.

***Index Terms*—Demodulation, disk drives, rotor position, synchronous integration.**

I. Introduction

With continuous effort to increase the areal density in hard disk drives (HDD), the performance requirements for spindle motor drive system become stringent and the highly accurate position feedback information of the motor is more and more important in both product and HDD production [1]. This motivates the exploration of the position sensing device which is precise and can withstand for vibration and environment changes.

Different kinds of position sensors are available depending on the required performance criteria. Resolver is one of the most promising sensors which can give absolute position angles with high accuracy. This sensor has the electromagnetic (EM) structure resembles an electric motor and works as a rotating transformer [2].

In a resolver, the primary winding which is energized by a high frequency alternating voltage resides on the rotor, and the two secondary windings which are in quadrature position locate on the stator giving the sensor outputs; see Fig. 1.

Since both the motor and sensor have the similar characteristics and materials, embedding the sensor in the motor is possible. The objective of this study is not about the design of the embedded sensor but on the decoding process of sensor outputs to obtain the rotor position. Several methods based on hardware and software approaches for decoding the angular position are reported in literatures [3]–[8]. The latter approach is more favorable because it is flexible and can be implemented using the existing digital signal processor (DSP) for motor control. Research works on software based methods can be found in [5]–[8]. Most of them aimed to improve the accuracy and to find simple and cost effective ways for implementation. The review of related works is provided in next section.

This study proposes a simple demodulation method which uses the synchronous integration to recover the envelopes of the modulated sensor signals. The method has the advantage of minimizing the noise effect and thus it improves the accuracy. In addition, the accuracy of the proposed method is not affected by the phase shift between the sensor inputs and outputs which is contributed by resistance of sensor windings.

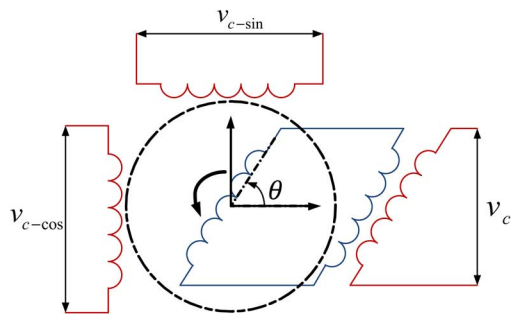

Fig. 1. EM structure of resolver.

II. Sensor Operation and Demodulation

When an excitation or carrier signal, $v_c(t) = V_c \sin(\omega_c t)$, is supplied to the sensor input winding, the two sensor outputs can be given by

$$\begin{cases} v_{c-\sin}(t) = gV_c \sin[\theta(t)] \sin(\omega_c t) \\ v_{c-\cos}(t) = gV_c \cos[\theta(t)] \sin(\omega_c t) \end{cases} \quad (1)$$

where g is the transformation ratio, ω_c is the angular frequency of the excitation signal. The illustration of the three signals is given in Fig. 2, where, the amplitude "gV_c" is set at 1 and the rotor is at a certain constant speed. The above equation is valid for the operations where the carrier frequency is relatively higher than the rotor frequency. Otherwise the quadrature components generated by the speed voltage should be included in (1) [9]. As the HDD spindle speed is typically around 300 Hz and the carrier frequency with 5 ~ 20 kHz, the expression is accurate enough for the proposed method.

The position angle may be computed from the ratio of the demodulated outputs as

$$\theta(t) = \tan^{-1} \frac{gV_c \sin[\theta(t)]}{gV_c \cos[\theta(t)]} \quad (2)$$

Manuscript received November 29, 2012; revised January 30, 2013; accepted January 30, 2013. Date of current version May 30, 2013. Corresponding author: N. L. H. Aung (e-mail: Nay_Aung@dsi.a-star.edu.sg).

Color versions of one or more of the figures in this paper are available online at http://ieeexplore.ieee.org.

Digital Object Identifier 10.1109/TMAG.2013.2245316

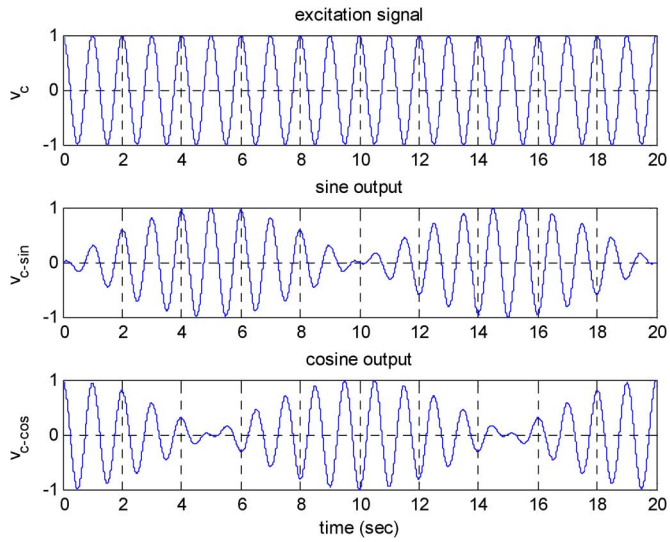

Fig. 2. Sensor input and outputs.

In order to retrieve the angle, two main tasks are involved: 1) demodulation and 2) extracting the angle from the demodulated quadrature signals. In communication discipline, the kind of modulation encountered here is used in Double-sideband suppressed-carrier transmission (DSB-SC) and the suggested demodulation technique for retrieving the information is based on coherent product detection or frequency shifting method followed by low pass filtering [10]. This method requires the synchronized carrier signal which is in phase with the modulated signals. If there is any phase shift between carrier signal and modulated signals, the demodulated output will be scaled by a constant.

Another approach for demodulation is the synchronous peak detection which samples the modulated signals at the carrier's peaks. In [5], this method is employed to demodulate the sensor signals by generation of a pair of quadrature carrier signals. The sampling instants are identified by zero crossing detection of the 90° phase shifted noise free carrier signal. This method is simple and attractive since it can demodulate the signal without any delay. However the accuracy of the sampled values is prone to the noise. In addition, the method neglects the phase shift between input and outputs due to resistance of the sensor windings. This method is often viewed as an under sampling method as the sampling frequency is lower than the Nyquist rate when the modulated signals are sampled.

In order to suppress the noise effect, the common approach is to use the filters. A comprehensive approach of synchronous peak detection by oversampling with taking into account of noise is presented in [6]. This approach uses a band pass filter followed by decimation. For a linear-phase finite impulse response (FIR) filter with N-taps, the delay can be expressed by $(\mathrm{N}-1)/(2.\mathrm{f_s})$, where $\mathrm{f_s}$ is the sampling frequency. The delay introduced by the filter is later compensated in the angle computation in that study. The influence of noise is reasonably reduced using this approach.

III. Proposed Method

The proposed method provides a new way to overcome the noise issue by over sampling the output signals and performing

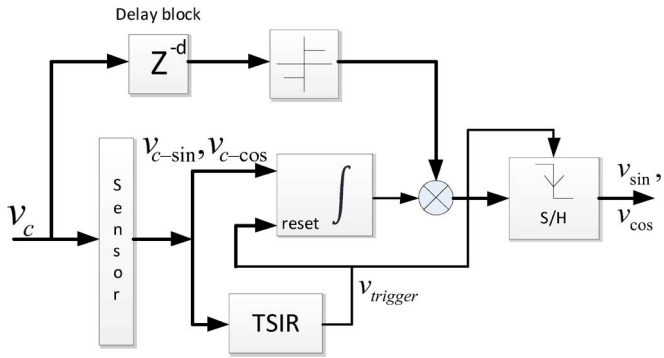

Fig. 3. Block diagram of the proposed method.

synchronous integration. The method is based on the assumption that during the half period of the carrier wave, the change in position signal is negligible or constant. During this interval, (1) can be expressed as

$$\begin{cases} v_{c-\sin}(t)\big|_{\theta=const} = G_1 \sin(\omega_c t) \\ v_{c-\cos}(t)\big|_{\theta=const} = G_2 \sin(\omega_c t) \end{cases} \tag{3}$$

Then the demodulation work is reduced to a simple amplitude detection task with a known frequency, i.e., finding G_1 and G_2. In practice the sensor signals are usually contaminated by the noise. Therefore, among the various methods available for amplitude detection, the integration method is chosen not only to obtain the amplitude but also to suppress the noise effect. The integration method thus determines the amplitudes as follows:

$$\begin{cases} G_1 = 0.5\omega_c \int_{t_0}^{t_n} v_{c-\sin}(t)\big|_{\theta=const} dt \\ G_2 = 0.5\omega_c \int_{t_0}^{t_n} v_{c-\cos}(t)\big|_{\theta=const} dt \end{cases} \tag{4}$$

where $\omega_c t_0 = \theta_0$, $\omega_c t_n = \theta_n$ and $\theta_n - \theta_0 = \pi$. To obtain G_1 and G_2 accurately we need the synchronous integration here. It means that the integration start and stop must be synchronized with the in-phase carrier signal. As there is usually a phase shift between the sensor input or the generated carrier and the outputs, the available sensor input signal is not used for synchronization. A method to recover the carrier signal from the sensor outputs is therefore devised in the proposed solution.

The block diagram of the synchronous integration scheme is given in Fig. 3. The triggering signal for integration reset (TSIR) is generated by detecting the zero crossings of two sensor outputs. This triggering signal actually represents the recovered carrier signal in pulse form. The details of the implementation of TSIR are provided in Fig. 4.

The TSIR may be generated using either one of the sensor outputs by detecting their zero crossing points (ZCPs). However due to the noise effect, some of the ZCPs from either output are not reliable, especially the ZCPs around the region where the envelope amplitude is getting smaller. Both sensor outputs are therefore employed in TSIR generation in conjunction with switching logic to produce an accurate triggering signal by comparing the amplitudes of modulated signals.

When doing comparison, each comparator's reference value is set to be the amplitudes of the position signal when the rotor is at $\pi/4$ radian. If one of the signal amplitude is greater than the reference value, the comparison result from this signal is

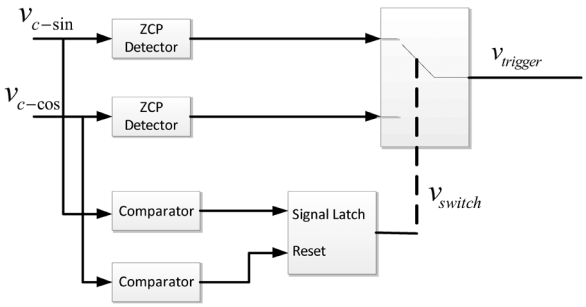

Fig. 4. TSIR generation.

latched until the other signal resets it. The switch waveform and its respective inputs are shown in Fig. 5.

The switching logic operates as follows: when $\mathrm{v_{switch}}$ is high, the triggering signal is chosen from ZCPs of $\mathrm{v_{sin}}$, otherwise the triggering signal is selected from ZCPs of $\mathrm{v_{cos}}$. Thus the synchronous integration is carried out depending on the triggering signal input.

In fact, the assumption of the position signal being constant during the half carrier period can be relaxed. Consider the rotor is at speed of ω rad/s. The modulated signals are

$$\begin{cases} v_{c-\sin}(t) = G_{\max}\sin(\omega t)\sin(\omega_c t) \\ v_{c-\cos}(t) = G_{\max}\cos(\omega t)\sin(\omega_c t) \end{cases}. \tag{5}$$

If the integration is carried out as before

$$\begin{cases} I_1 = \int_{t_0}^{t_n} v_{c-\sin}(t)dt \\ I_2 = \int_{t_0}^{t_n} v_{c-\cos}(t)dt \end{cases} \tag{6}$$

where the period is defined as $(\omega_c \mathrm{t_n} - \omega_c \mathrm{t_0}) = (\theta_\mathrm{n} - \theta_0) = \pi$ with $\theta_0 = \mathrm{k}\pi$ for $\mathrm{k} = 0, 1, 2, 3\ldots$ If we consider the even numbers of k, (6) can be derived as

$$\begin{cases} I_1 = \frac{\omega_c G_{\max}}{\omega_c^2 - \omega^2}\left[\sin(\omega t_n) + \sin(\omega t_0)\right] \\ I_2 = \frac{\omega_c G_{\max}}{\omega_c^2 - \omega^2}\left[\cos(\omega t_n) + \cos(\omega t_0)\right] \end{cases}. \tag{7}$$

Applying trigonometric expansion and the definition of integration period, $\omega_c \mathrm{t_n} = \theta_\mathrm{n}$ and $\omega_c \mathrm{t_0} = \theta_0$, (7) can be expressed by

$$\begin{cases} I_1 = \frac{2\omega_c G_{\max}}{\omega_c^2 - \omega^2}\left[\sin\left\{\frac{\omega(t_n+t_0)}{2}\right\}\cos\left\{\frac{\omega}{\omega_c}\frac{(\theta_n-\theta_0)}{2}\right\}\right] \\ I_2 = \frac{2G_{\max}}{\omega_c^2 - \omega^2}\left[\cos\left\{\frac{\omega(t_n+t_0)}{2}\right\}\cos\left\{\frac{\omega}{\omega_c}\frac{(\theta_n-\theta_0)}{2}\right\}\right] \end{cases} \tag{8}$$

It can be observed that the common factor in the bracket of (8) is a fixed value for a constant speed operation. This factor will be cancelled out due to the ratio effect in angle computation. In addition, considering the fact that $\omega_c \gg \omega$, (8) can be simplified as

$$\begin{cases} I_1 \approx \frac{2G_{\max}}{\omega_c}\sin\left[\frac{\omega(t_0+t_n)}{2}\right] \\ I_2 \approx \frac{2G_{\max}}{\omega_c}\cos\left[\frac{\omega(t_0+t_n)}{2}\right] \end{cases}. \tag{9}$$

The estimated amplitudes in this period can be obtained by

$$\begin{cases} G_{sr}(\theta_{mid}) = 0.5\omega_c I_1 = G_{\max}\sin(\theta_{mid}) \\ G_{cr}(\theta_{mid}) = 0.5\omega_c I_2 = G_{\max}\cos(\theta_{mid}) \end{cases} \tag{10}$$

where $\theta_{\mathrm{mid}} = \omega(\mathrm{t_0} + \mathrm{t_n})/2$. The integration therefore effectively results in the position signal amplitudes at the middle of the integration period with a quarter of the carrier period delay. This delay can be compensated when the position angle is computed using the tracking observer based on PI controller.

The integration results in both positive and negative amplitudes depending on the odd and even number of k in $\theta_0 = \mathrm{k}\pi$. These amplitude values must be corrected according to the actual shape of the corresponding envelope. The carrier signal and sensor outputs have the phase relationship as shown in Fig. 6 and Table I.

According to the phase relationship, the correct envelope amplitudes can be retrieved by multiplying the integrated results with the sign of the carrier signal amplitude. Since the integration is completed at the end of the half the carrier period, taking carrier sign at this instant is not suitable. Therefore the carrier signal is delayed approximately $\pi/4$ period before sign extraction to ensure the right sign. This delay can be adjusted to take into account of the phase shift and it is not necessarily to be exactly $\pi/4$ period. In this way, the correct envelope is retrieved making the demodulation process reasonably immune to the noise effect.

IV. Position Angle Computation

Once the senor outputs are demodulated, the position angle can generally be computed using two approaches. One is the direct computation of trigonometric ratio as described in (2).

Another approach of finding the position angle is based on the trigonometric identity of sine function;

$$\sin(\theta - \hat{\theta}) = \sin\theta\cos\hat{\theta} - \cos\theta\sin\hat{\theta} \tag{11}$$

where θ is the actual position angle and $\hat{\theta}$ is the estimated position angle. When the difference between the two angles is small enough, we can use the small angle approximation which will give us

$$\sin(\theta - \hat{\theta}) \approx (\theta - \hat{\theta}) = \varepsilon. \tag{12}$$

This error signal ε is fed into the control loop that forces the error to become zero. In other words, the control loop drives the estimated angle to equal the actual angle. The angle computation of such approach is commonly described as the tracking observer approach and the control loop is realized by a PI controller with an integrator to achieve the zero steady state error. This method inherently gives both the velocity output and the filtered position signal. Due to the filter action of the control loop this method has an advantage of being more robust to noise.

As presented, the proposed method has a constant time delay of quarter of the carrier period. This delay can be compensated adapting the technique in [6], where the angle is computed with the tracking observer by delaying one sample in the feedback path.

According to the proposed scheme, the control loop shown in Fig. 7 processes the input signal two times in one carrier period since two amplitude values are available in that period. The clock for the control loop is the same as TSIR but with a quarter carrier period delay to make the total delay to be a half carrier period. This delay can then be compensated by one sample delay, i.e., a half carrier period delay, in the feedback loop. The performance of the control loop can be specified by adjusting the gains in the PI controller and the integrator.

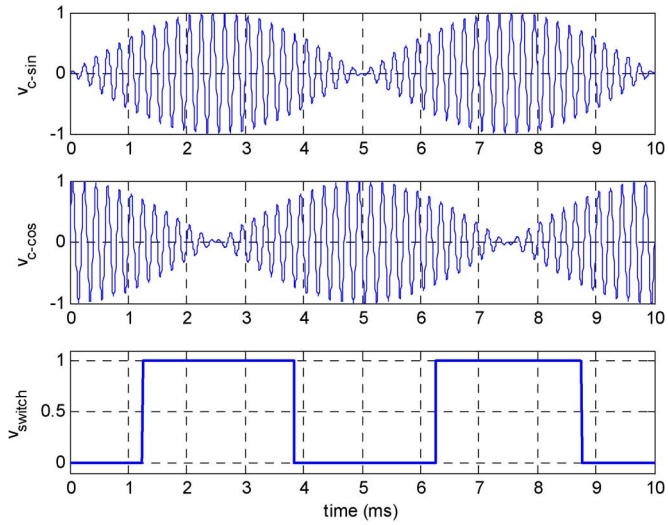

Fig. 5. Switching signal with respect to sensor outputs.

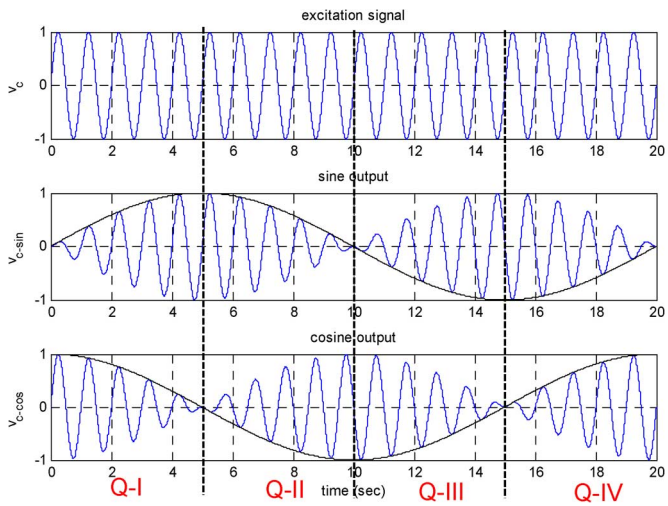

Fig. 6. Four quadrants of the signals.

TABLE I
PHASE RELATIONSHIP

	v_c & $v_{c-\sin}$	v_c & $v_{c-\cos}$	$v_{\sin}(env)$	$v_{\cos}(env)$
Q-I	In phase	In phase	+ive	+ive
Q-II	In phase	Out phase	+ive	-ive
Q-III	Out phase	Out phase	-ive	-ive
Q-IV	Out phase	In phase	-ive	+ive

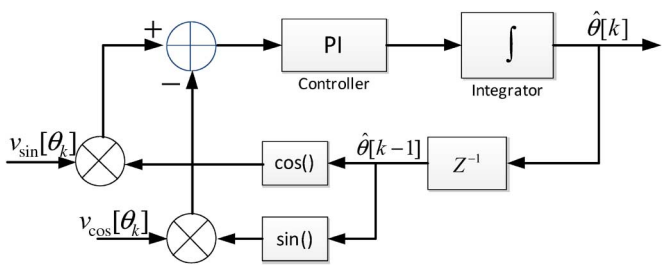

Fig. 7. Position angle computation.

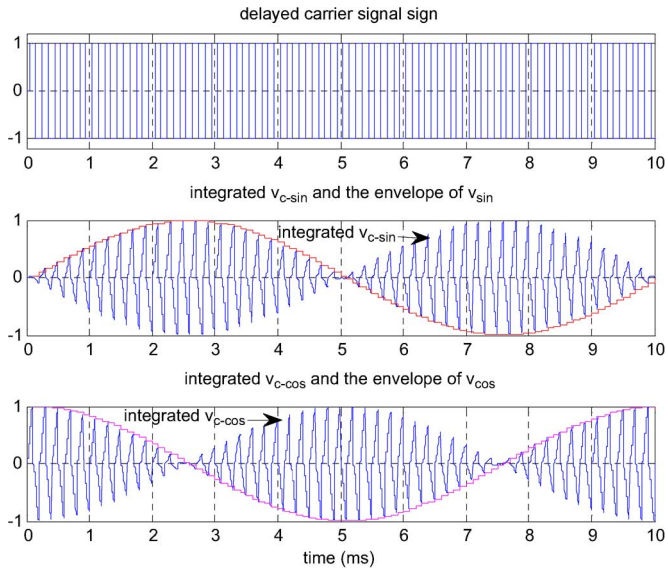

Fig. 8. Demodulation by proposed method.

V. Simulation and Experimental Results

To validate the effectiveness of the proposed method, simulation is carried out on SIMULINK platform. Trapezoidal numerical integration is applied in implementation and (4) is transformed into

$$\begin{cases} G_1 = \frac{\pi f_s}{2N} \sum_{k=1}^{N} v_{c-\sin}[k] \Big|_{\theta=const} \\ G_2 = \frac{\pi f_s}{2N} \sum_{k=1}^{N} v_{c-\cos}[k] \Big|_{\theta=const} \end{cases} \tag{13}$$

where $N = f_s/2f_c$ with f_s = sampling frequency and f_c = carrier frequency. Thus, N is restricted to be an integer value and it represents the number of samples being taken in half the carrier period. The expression implies that the integration is in fact a simple averaging which can easily be realized in DSPs.

The first simulation result is provided in Fig. 8 to illustrate the principle of operation in the proposed method using the parameters: rotor speed, 6000 rpm, carrier frequency, 5 kHz with unit amplitude, sampling frequency, 250 kHz and the transformation ratio, 1.

Fig. 8 displays the continuous integration results of both sensor outputs and their corresponding envelopes which are recovered by multiplying the integrated values at the end of integration with the sign of the delayed carrier signal. It can be seen that the proposed method perfectly demodulates the sensor outputs as described.

In order to investigate the noise effect, an additive white Gaussian noise with SNR 40 dB is added to the sensor outputs while the rotor speed is 12000 rpm. The simulated results showed in Fig. 9 gives the comparison of the proposed method with the other two methods: the synchronous peak detection method and the band pass FIR filter with decimation method.

Synchronous peak detection uses the 90° phase shifted carrier signal for sampling and its sample rate is the same as the carrier frequency. For the band pass filtering method, the sample rate is chosen to be 40 kHz and the down sampling takes every 8th sample from the 17-tap filter's output. So the equivalent sample

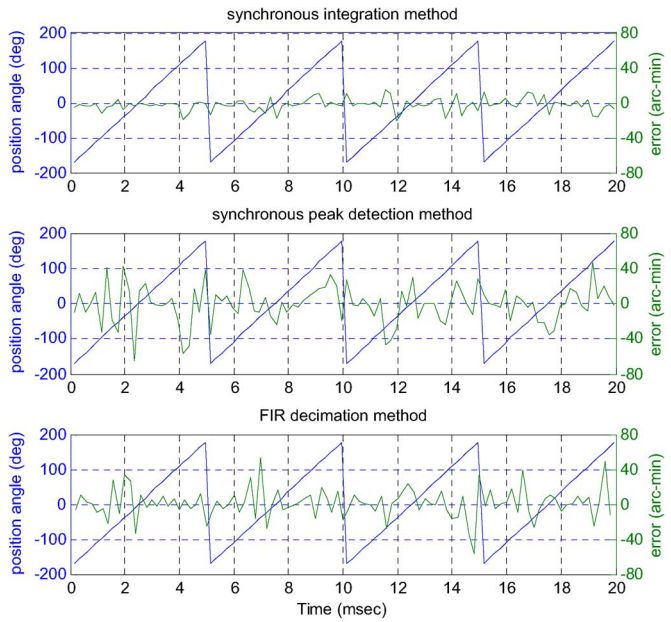

Fig. 9. Position angle and error at SNR 40 dB.

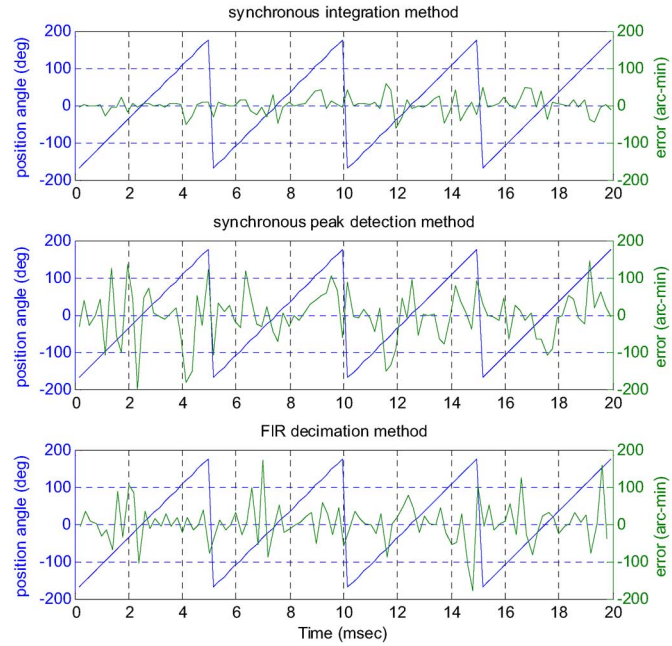

Fig. 10. Position angle and error at SNR 30 dB.

rate is also the same as the carrier frequency for this method. All three methods are compared against with the noise free sensor outputs. From the comparison shown in Fig. 9, it can be found that peak position error is around 15 arc-min for the integration method while it is around 40 arc-min for the other two methods. It is observed that the proposed method can significantly average out the noise effect among three methods. It can be argued that if a higher sample rate is used for FIR decimation method, position error due to noise can be further reduced. However, the higher sample rate requires more taps and it in turns increases the computation load as more multiplications involve.

It should be noted that the proposed method has the position resolution two times higher than the others as both the positive and negative amplitudes in one carrier period are captured. The other two methods can achieve the same resolution if the effective sample rate is increased twice by sampling both positive and negative peaks, and the phase relationship is applied as the proposed method.

To see the performance of the propose method against the higher noise level, the same simulation setup is used with SNR 30 dB. The result shown in Fig. 10 proves that the proposed method is more immune compared to the other two methods as before. Regarding the phase shift effect on the angle computation, a simulation is carried out for a condition where there is a phase shift of 10° between the senor input and outputs while the noise is kept at SNR 40 dB. The simulation results shown in Fig. 11 highlights that the phase shift has insignificant effect on the angle computation for integration method.

The performance of the three methods in terms of root mean square error (RMSE) is provided in Table II. It shows that the proposed method can efficiently suppress the noise effect yielding more accurate position results. RMSE is computed by

$$RMSE = \sqrt{\frac{1}{T}\int_0^T \left(\theta(t) - \hat{\theta}(t)\right)^2 dt} \qquad (14)$$

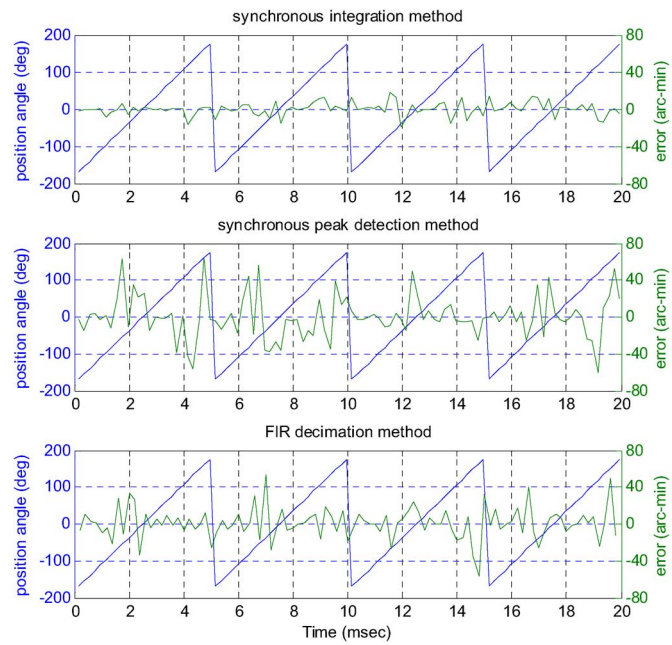

Fig. 11. Position angle error at SNR 40 dB with reference phase shift of 10°.

TABLE II
COMPARISON OF RMSE FOR SIMULATION RESULTS

	Integration method	Peak detection method	FIR method
SNR 40dB (Fig.9)	7.0254	20.8740	16.7823
SNR 30dB (Fig.10)	22.3768	65.8297	52.8975
SNR 40 dB & phase shit 10°(Fig.11)	7.0254	27.4640	16.7823

where T is the simulation time.

Experiments are also carried out by assembling a resolver to the shaft of a spin-stand. The excitation signal at 5 kHz is

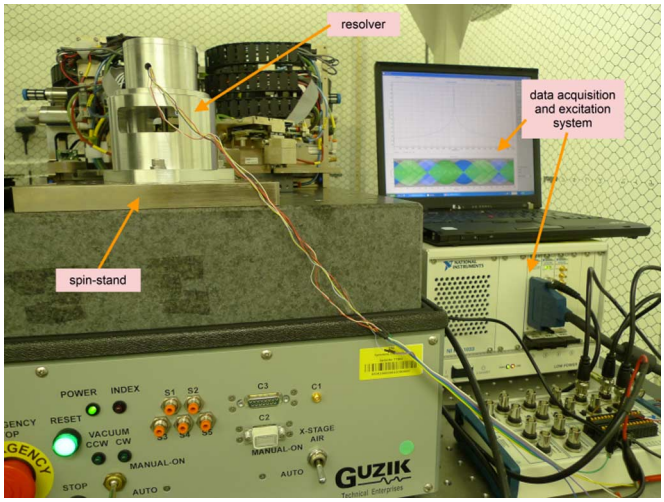

Fig. 12. Experiment setup.

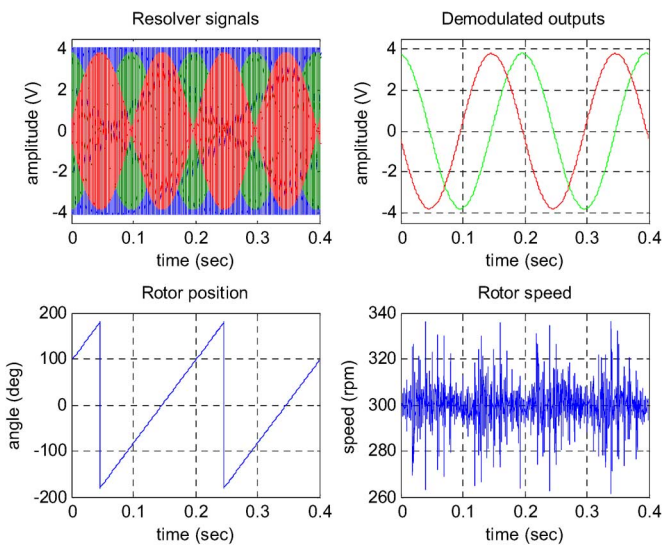

Fig. 13. Rotor position detection at 300 rpm.

generated by NI PXI-5406 and sensor signals are acquired by NI PXI-6133. The experiment setup is shown in Fig. 12. Similar to the simulation settings, the sampling frequency is set to 250 kHz. The rotor position detection is performed when the spindle motor is at speed of 300 rpm and 4200 rpm respectively. The results from the processing of acquired data on SIMULINK platform using the proposed method are shown in Fig. 13 and Fig. 14. Rotor position is computed directly with inverse tangent approach and the speed is derived from the derivative of the position angles. It can be observed that the proposed method works effectively in rotor position detection.

VI. Conclusion

Accurate rotor position detection is essential for the high performance drive control in HDD. The study proposes a new demodulation method to process the amplitude modulated signals

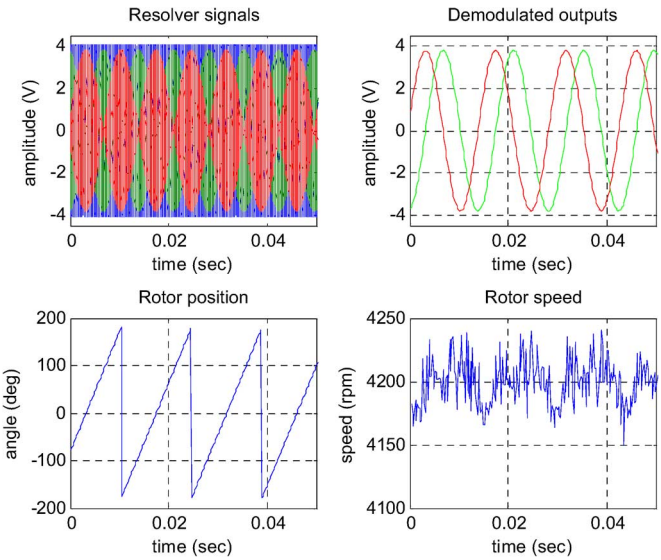

Fig. 14. Rotor position detection at 4200 rpm.

from a resolver. The new method performs the demodulation by a simple amplitude detection approach. It uses only the available signals to operate the sensor and performs the synchronous integration to demodulate the signals. The computational effort requirement is less compared to the common filtering methods. The method presented can retrieve position signal with high resolution, and makes the angle decoding robust against noise with reasonable accuracy, and all these are important for HDD with ultrahigh data recording density, and many other applications.

References

[1] C. Bi, "Hard disk drive spindle motor system design for data recording with ultrahigh TPI," *IEEE Trans. Magn.*, vol. 45, no. 11, pp. 5123–5128, Nov. 2009.

[2] , G. Boyes, Ed., *Synchro and Resolver Conversion*: Analog Devices Inc., 1980.

[3] M. Benammar, L. Ben-Brahim, and M. A. Alhamadi, "A novel resolver-to-360° linearized converter," *IEEE Sensors J.*, vol. 4, no. 1, pp. 96–101, Feb. 2004J.

[4] L. Ben-Brahim, M. Benammar, and M. A. Alhamadi, "A resolver angle estimator based on its excitation signal," *IEEE Trans. Ind. Electron.*, vol. 56, no. 2, pp. 574–580, Feb. 2009.

[5] S. Sarma, V. K. Agrawal, and S. Udupa, "Software-based resolver-to-digital conversion using a DSP," *IEEE Trans. Ind. Electron.*, vol. 55, no. 1, pp. 371–379, Jan. 2008.

[6] M. Staebler, "TM320F240 DSP solution for obtaining resolver angular position and speed," Texas Instrument Application Report SPRA605 Feb 2000 [Online]. Available: www.ti.com/cn/cn/lit/an/spra605/spra605.pdf

[7] A. O. Di Tommaso and R. Miceli, "A new high accuracy software based resolver-to-digital converter," in *Industrial Electronics Society, 2003. IECON '03*, vol. 3, pp. 2435–2440, Vol. 3.

[8] D. A. Khaburi, "Software-based resolver-to-digital converter for DSP-based drives using an improved angle-tracking observer," *IEEE Trans. Instrum. Meas.*, vol. 61, no. 4, pp. 922–929, Apr. 2012.

[9] D. C. Hanselman, "Techniques for improving resolver-to-digital conversion accuracy," *IEEE Trans. Ind. Electron.*, vol. 38, no. 6, pp. 5101–504, 1991.

[10] S. Haykin, *Communication Systems*, 4th ed. New York: Wiley, 2001.